

Experimental validation of a FEM constitutive model for an innovative L-PBF AM Metal-Matrix-Composite

Original

Experimental validation of a FEM constitutive model for an innovative L-PBF AM Metal-Matrix-Composite / Sesana, R., Delprete, C., Belen Fraga, L., D'Hers, S., Crachi, M.. - (2025). (21st INTERNATIONAL CONFERENCE ON EXPERIMENTAL MECHANICS Bologna (ITA) 6-11 July, 2025).

Availability:

This version is available at: 11583/2996647 since: 2025-01-16T20:41:55Z

Publisher:

ICEM

Published

DOI:

Terms of use:

This article is made available under terms and conditions as specified in the corresponding bibliographic description in the repository

Publisher copyright

(Article begins on next page)



Experimental validation of a FEM constitutive model for an innovative L-PBF AM Metal-Matrix-Composite

Matteo Crachi^a, Raffaella Sesana^a, Cristiana Delprete^a, Leila Belen Fraga^b, Sebastian D' hers,

^aDIMEAS Politecnico di Torino Corso Duca degli Abruzzi 24 10129 Torino (TO) Italy

^bInstituto Tecnológico de Buenos Aires Iguazu 341 C1437 Cdad. Autónoma de Buenos Aires Argentina

Correspondence to matteo.crachi@polito.it

1. Introduction

One of the most critical components of high performance bi-propellant Liquid Rocket Engines are the thrust chambers. To keep temperature controlled and preheat the propellant, the use of regenerative cooling is widely used. The propellant is injected, mixed, and combusted inside to produce high-pressure and high-temperature gases. These gases exert extreme thermal loads on the walls of the chamber, which can easily exceed the melting point of conventional materials. To prevent failure, regenerative cooling channels are integrated into the walls allowing a portion of the propellant to flow through and absorb the heat.

Additive manufacturing (AM) is a process that involves creating three-dimensional objects by adding layers of material. It makes possible to manufacture thrust chambers, as single, integrated component, reducing the number of parts and eliminating the need for complex assembly processes.

Material selection affects the performance, reliability, and safety of the thrust chamber. To meet specific requirements, several factors must be taken into consideration. Some characteristics are thermal conductivity, thermal expansion, mechanical strength, and corrosion resistance to withstand the environment created by the combustion products [1]

Copper alloys offer high thermal conductivity and good corrosion resistance, crucial properties for the thrust chambers where harsh chemicals are involved. However, these alloys alone may not possess the required mechanical strength and stiffness needed. To overcome this limitation, high strength steel or nickel alloys are often used in conjunction with copper alloys to create Metal Matrix Composites (MMC). The combination of these materials can be tailored to have the necessary mechanical properties to withstand the high pressure and loading conditions experienced during rocket engine operation [2].

The primary aim of the present research is to delve into the mechanical properties of an innovative MMC. To address this, the present in-depth study was developed by means of Finite Element Analysis (FEA) approach, allowing to calibrate the behavior and specific properties of the Cu17-4PH MCC by means of nano indentation to compute the young modulus.

2. Materials and methods

In the present research, the investigated MMC has a custom composition of 65% copper and 35% 17-4PH stainless steel prior to the manufacturing process. Specimens for experimental testing were manufactured by means of a Concept Laser M2 machine. Process parameters were set according to the internal research group know-how, findings from previous research projects [4], and the similarity between the properties of the composites.

The research plan is composed of three parts: experimental tensile monotonic testing, nano hardening tests and numerical simulation of tensile monotonic testing. Experimental tensile tests provide stress-strain curves where the strain is measured both globally on the whole specimen and locally within the microstructure of the MMC via Direct Image Correlation. Tests are run in a SEM fixture to allow the observation of microstructural distribution of strain on MMC surface by means of DIC acquisition and analysis. This procedure aims at investigating the microstructural behavior and composition and at analyzing the Representative Volume Element (RVE) dimensions to be used in the numerical simulations. The numerical analysis replicates the tensile test with a focus on the calibration of the constitutive material model for MMC based on microstructural component distribution and to mimic the contribution of the diverse components of MMC to the global straining behavior. The calibrated constitutive models, focusing on the young modulus are then compared with the extrapolated ones by means of local nano hardness tests.

3. Results and conclusions

The FE mesh is exported to a commercial FEM software solver and employed to simulate the elastoplastic behavior of the microstructure, as shown in Figure 2, where the boundary conditions and loads are indicated. A distributed force designed to achieve 3000 N, the maximum load observed in the load-displacement curves, in 100 incremental steps, is imposed at the top of the mesh.

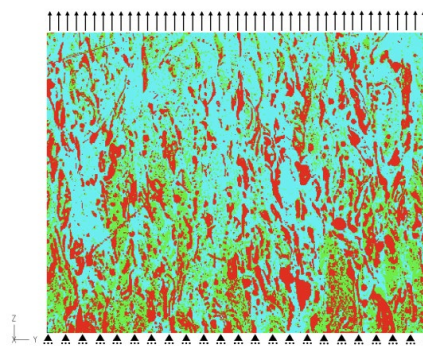


Figure 2 - FE mesh depicting the applied loads and boundary conditions used for the tensile test simulation

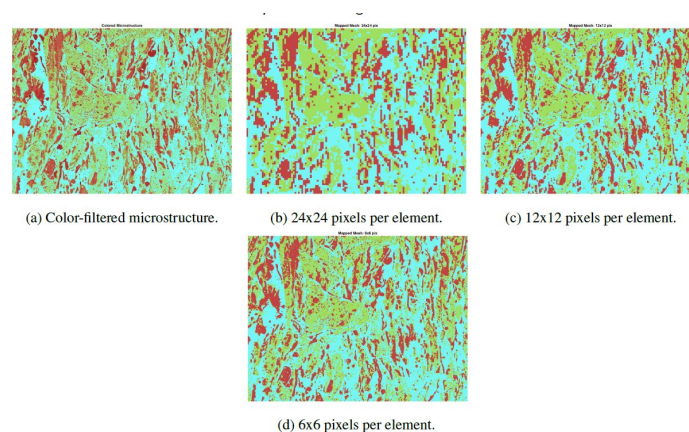


Figure 2 - FE mesh depicting the applied loads and boundary conditions used for the tensile test simulation

Cracks within a material microstructure can dramatically deviate the strain-stress curve from its typical trajectory. Serving as stress concentrators, these cracks intensify the local stress level, precipitating an earlier commencement of plastic deformation and ultimately, leading to fracture at reduced overall stress levels. The material at the crack tip is subjected to significantly higher stress than the remaining material, triggering localized plastic deformation, propagation of the crack, and eventual failure.



The results garnered from simulations conducted with FEM commercial software will be presented and discussed, reporting Specimen 2 results as an example.

To accurately calibrate the mechanical properties of the MMC, a series of simulations were conducted, during which the strain hardening modulus and yield strength were systematically adjusted to align with the strain-stress curve derived from the tensile test. The strain maps obtained from FE simulation are compared to the experimental ones obtained from DIC during testing, for each specimen. Subsequently, the material properties can be adjusted. This process allows for a congruence in the elastic and plastic region across DIC and FE. The conclusive results of these simulations are illustrated in Figure 3. The curve overlapping demonstrates the accuracy of the simulation in replicating the physical test outcomes. Although the yield strength of the mix does not adhere to the rule of mixtures, the strain hardening modulus does. This property was calculated using the initial MMC proportions of 65% Cu and 35% 17-4PH.

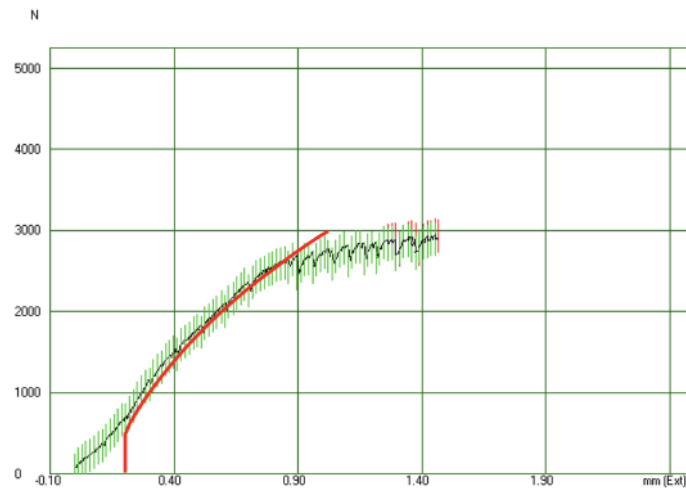


Figure 3 - Comparison of Strain-Stress curves obtained from tensile test (black) and FE simulation (red).

The two curves overlap in the linear range. The mismatches at the beginning can be attributed to settlement issues, which are also reflected in the concavity of the strain-stress curve derived from the test. The tail end of the curve does not match due to the failure of the MMC caused by crack propagation in the interfaces, as illustrated in Figure 4. Crack propagation is not included in numerical analysis.

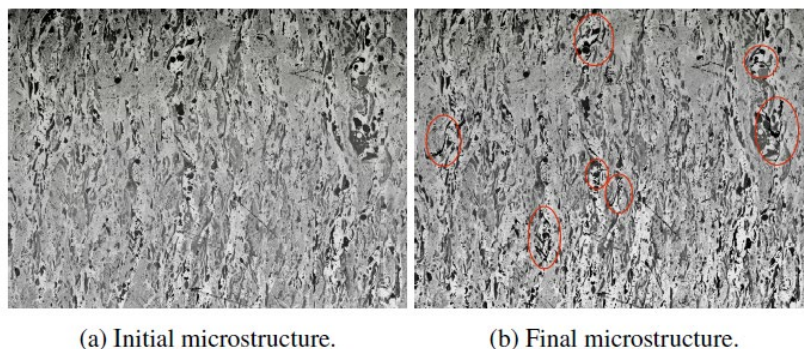


Figure 4 - Comparative microstructural analysis at the onset (left) and conclusion (right) of the tensile test, highlighting the effect of crack propagation.

The simulated curve would approach a horizontal asymptote if the stainless steel would undergo full plastic deformation. However, in Figure 5 the strain-stress bilinear behavior for each of the three materials comprising the modeled MMC is illustrated. The strain-stress curve is obtained by choosing an exemplary element from each material and extracting the data calculated at the Gauss points.

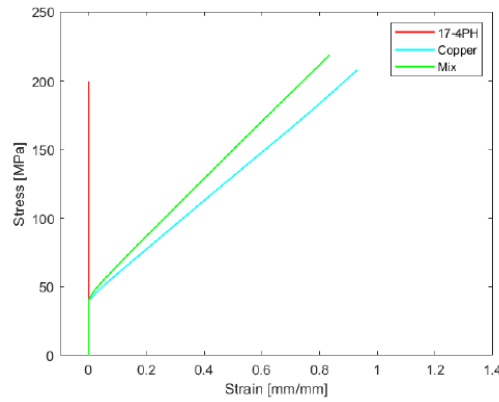


Figure 5 - Strain-stress curves for constituent materials of the MMC under tensile loads

The mean strain and its space-wise distribution is compared between the FEA and the DIC ones, as depicted in Figure 6 in the plastic field. The findings, as detailed in Table 2, confirm the validity of the DIC software for the intended analysis in this research. As illustrated in Figure 7, the strain maps from both analyses correspond in a zone free from cracks and porosity. A calculation of the mean accumulated plastic strain is made using both the DIC and numerical solver. The results of this analysis are presented in Table 2. An error margin of nearly 2% is recorded, which is considered within an acceptable range.

Model	e_{xx}	e_{xy}	e_{yy}
DIC	-2.382e-3	-1.096e-5	6.958e-3
FEA	2.222e-3	-1.250e-5	.900e-3
Error [%]	7.20	12.32	8.41

Table 2 - Comparative analysis of mean strain values derived from both DIC and FEA.

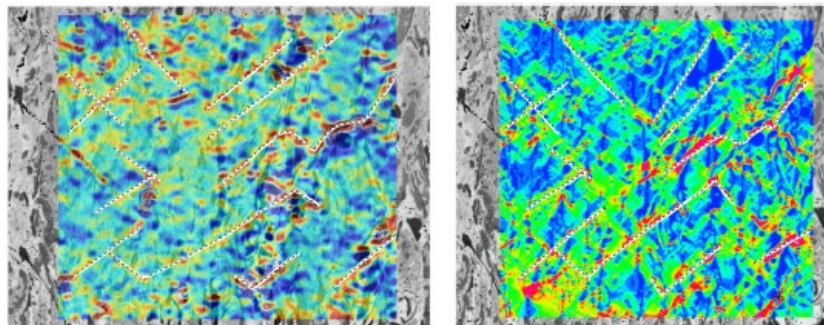


Figure 6 - Comparison of strain maps from DIC (left) and FEA (right) revealing similar patterns in strain distribution

In Figure 7 the strain pattern shows the typical characteristic of shear bands in metallic materials under high strain, which typically form a zigzag or wavy geometric pattern. The angle at which this zigzag pattern manifests in shear bands can be variable, contingent on the material and prevailing conditions. However, it forms at a 45° angle.

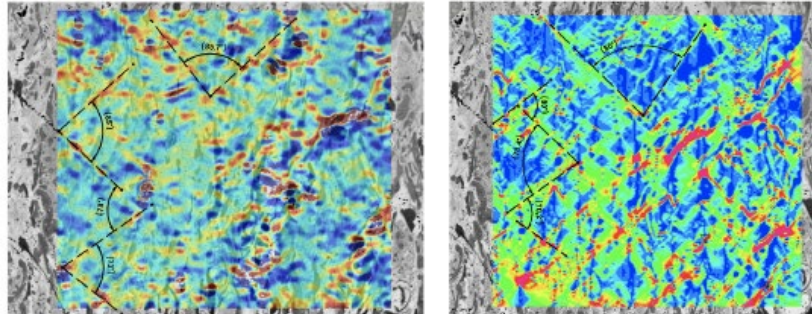


Figure 7 - Shear bands drawn on top of strain maps from DIC (left) and FEA (right).

	FEA	DIC	Relative Error
Mean Accumulated Plastic Strain	0.04639920	0.04545096	2.086%

Table 2 - Results of the mean accumulated plastic strain calculated with both DIC and FEA.

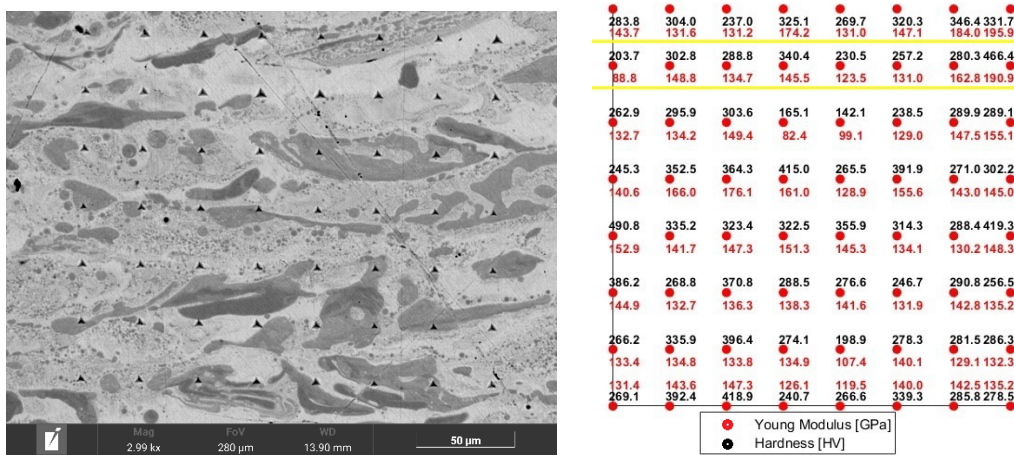


Figure 8 – Nano hardness map and Young Modulus computation

This project aimed to determine the mechanical properties of a MMC through the analysis of SEM images and nano indentation tests. The project's main objectives were successfully achieved with precision and accuracy. The strain-stress curve obtained from the tensile test of Specimen 2 was successfully corroborated using FEA and the calibrated Young Modulus validated by means of nano hardness, demonstrating a strong alignment with the rule of mixtures. This finding validates the effectiveness of FEA in accurately modelling the mechanical behavior of MMCs under tensile load by using the rule of mixtures as a first approach. The comparison of strain map distribution between DIC and FEA further reinforced the accuracy of the models used, with the mean accumulated plastic strain from both methods showing an

acceptable error of almost 2%. This close match underscores the reliability of both DIC and FEA in mapping strain distribution in MMCs. For future work and in order to gain a more comprehensive understanding of the mechanical properties and behavior of the MMC, it would be recommended to adjust and calibrate these properties through multiple tensile tests. This would ensure a more accurate and reliable understanding of the material behavior. In terms of fracture mechanics, a deeper and more detailed analysis could be obtained by calculating the stress intensity factor for multiple crack tips in an interface. This would give a more complete picture of how the MMC responds to stress and fails. Additionally, it would also be beneficial to employ a different method other than CTOD for these calculations. One such method that could be used is computational simulations with the Extended Finite Element Method (X-FEM).

5. References

- [1] Michele Ferraiuolo, Michele Perrella, Venanzio Giannella, and Roberto Citarella. Thermal–Mechanical FEM Analyses of a Liquid Rocket Engines Thrust Chamber. *Applied Sciences*, 12(7):3443, March 2022.
- [2] Andrea El Hassanin, Fabio Scherillo, Umberto Prisco, Raffaele Sansone, and Antonello Astarita. Selective laser melting of Cu-inconel 718 powder mixtures. *Journal of Manufacturing Processes*, 59:679–689, November 2020.